2003

How realistic is the high frequency signal of a 0.1° resolution ocean model?

Tokmakian, Robin

To appear in , xxxx, x, 2002

How realistic is the high frequency signal of a 0.1° resolution ocean model?

Robin Tokmakian and Julie L. McClean

Department of Oceanography, Naval Postgraduate School, Monterey, California

Abstract.
This paper describes the results from a comparative wavelet analysis of a 0.1°, 40-level Parallel Ocean Program model simulation of the North Atlantic with coincident in situ measurements of sea surface height (SSH) and temperature. The wavelet analysis is used to examine the realism of the surface's variability and its high frequency signals (less than a year). Along the coast, it shows that the model's simulated fields of SSH are realistic with the correlations to tide gauge measurements on the order of 0.8. The wavelet spectra show that the model replicates the observations' frequency space. Comparisons of the model's temperatures to temperatures from NOAA buoys north and south of the Gulf Stream show that, while not replicating the location of mesoscale features all the time, the model's energy in the strong mesoscale regions compares favorably to data. Due to the TOPEX/POSEIDON's (T/P) sampling, which requires large areal averages and because of the model's spontaneous eddy field, the evaluation of the simulation in the open ocean is less conclusive. The model does show similarities to the T/P data at high latitudes where the sampling by the sensor is denser and also on the eastern side of the basin with its lower mesoscale activity. Spatially, there are similarities in the amplitude of the signals between the model and the observations in areas with a significant signal in a given spectral band.

1. Introduction

The large scale, low frequency signal observed in nature is reproduced reasonably well in ocean models forced with realistic, daily varying momentum, heat, and freshwater fluxes [*Smith et al.*, 2000]. There has been little analysis of the realism of the high frequency components of the variability represented in an ocean model. *McClean et al.* [2002] describe a comparison of Eulerian and Lagrangian statistics between surface drifting buoys and an eddy-resolving ocean model, the same as used in the analysis presented in this paper. They found that typical time and length scales for these data are between 2-4 days and between 20 and 50 km. The model's scales show reasonable statistical agreement with these values. Differences were seen in the North Atlantic Current (NAC), the Canary Current, over the Mid-Atlantic Bight, and in places where the model's Gulf Stream is displaced to the south of the observed stream. This has been noted and discussed in *Smith et al.* [2000]. Additional examination of the realism of the high frequency band of a model is given in *Chao and Fu* [1995] using a low resolution (2°x 1°) primitive equation ocean model and only for a two year period. When comparing the simulated fields to the same two years of TOPEX/POSEIDON altimeter data, they find that there are large areas in the simulated fields which are coherent with the 20 to 100-day band observed by TOPEX/POSEIDON. They relate these changes to a barotropic response of the ocean to the wind forcing.

This paper discusses the results from wavelet analysis applied to an ocean model with 40 levels, 0.1° resolution forced with daily varying, realistic winds and a daily varying climatological heat flux. The modeled fields evaluated in this paper can be used to initialize either a similar model for prediction purposes or for providing boundary conditions for even higher resolution regional models. To use simulated fields for such purposes, the fields need to be qualitatively evaluated, not only at the annual and lower frequencies, but

also at high frequencies. Such an evaluation is performed in this paper using different sets of in situ measurements and using a technique which helps describe temporal changes. Rather than strictly looking at in situ data and simulated fields using first order statistics, we examine the temporal variation in the spectra of comparable fields. The ocean model is described first followed by the descriptions of the in situ data sets, and the analysis method that we have used (wavelet theory). The next three sections describe the results of the analysis performed on the model output and three different data sets: tide gauges, altimetry, and near surface temperatures from buoys. Current speeds were examined, but time series were not available for an extended temporal comparision and thus are not discussed. A discussion of the combined results follows including comments on how the analysis can be helpful in assimilating data for ocean state prediction efforts.

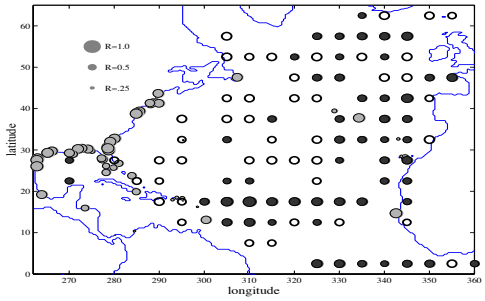

Figure 1. Map of correlations between tide gauges and model (gray dots) and between T/P 5°x 5° averages and model SSH fields (black dots/circles). For the the comparisons, the open circles have correlations between 0.4 and 0.5 and the black dots are greater than or equal to 0.5. The tide gauges are all gray dots. The values are all significant for the black dots and also for the tide gauges with correlations greater than 0.35

2. Description of the ocean model and in situ data sets

The ocean model whose high frequency signal is examined in this paper is the Parallel Ocean Program (POP) model. It has a resolution of 0.1° at the equator with 40 levels. It is configured for the North Atlantic basin; the domain is defined as 20S - 72N, 98W - 17E, which includes the Gulf of Mexico and the western Mediterranean Sea. It has a Mercator grid resulting in horizontal resolutions varying from 11.1 km at the equator to 3.2 km at the northern boundary. The horizontal spacing of this grid is less than or equal to the first baroclinic Rossby radius which results in eddies being reasonably well resolved up to approximately 50 degrees latitude. [*Smith et al.*, 2000, Fig. 1]. POP has an implicit free surface and includes mix layer dynamics [*Semtner and Chervin*, 1992, *Dukowicz and Smith*, 1994].

The simulation was forced with daily varying Naval Operation Global Atmospheric Prediction System (NOGAPS) winds for a period of six years [*McClean et al.*, 2002], 1993 through 1998. The heat flux also varied daily, but was a yearly climatology (monthly fields averaged for the period 1986-1988, [*Barnier et al.*, 1992]). Surface salinity is weakly restored to climatology. The *Large et al.* [1994] mixed layer formulation, K- Profile Parameterization (KPP), is active in this simulation. It was initialized from the *Smith et al.* [2000] run which was configured in the same manner but was forced with different winds and lacked a mixed layer. Three day averages of the prognostic variables (velocity x and y components, U,V; temperature, T; salinity, S; and sea surface height, SSH) were saved for the complete time period of the simulation.

Three in situ data sets have been used to evaluate the realism of the model. The first, and most robust set is the tide gauge data set from the University of Hawaii [*Kilonsky and Caldwell*, 1991] . A large number of the time series from coastal stations in this data set were collected over the entire period of the simulation. Daily averages of the sea level data set are used for comparisons to the model's SSH field. An inverse barometer contribution to the tide gauge SSH signal is removed so that direct comparisons can be made to the model fields which do not include surface forcing pressure. The contribution is determined using daily maps of sea level pressure. The tide gauge daily values were averaged to the center time of the model's three day averaged period. Based on *Tokmakian* [1996], Figure 1 shows a map of correlations (tide gauge stations are those shown in gray, black closed and open circles for the T/P comparisons) of the Atlantic time series with the model's SSH. Only stations with series longer than three years are shown. Because of the high frequency and localized sampling of the tide gauges, comparisons can be made between the model output and the data at frequencies as short as six days.

The second daily sampled data set we use is from a set of buoy temperature data provided by NOAA that are coincident with the model time period. We have chosen to

show two examples which are representative of many of the data/model pairs. Daily values are averaged every three days to match the sampled fields saved during the run. The model fields are sampled and averaged in an area within 60km of the location of the buoy.

The third set is a global data set, the TOPEX/POSEIDON altimeter's estimate of the SSH anomaly field. To examine frequencies at relatively high frequencies (20 days), it is necessary to average the 10-day repeat cycle data into bins over large areas (2°x 2°) to reduce the sampling error inherent in the widely spaced along track T/P measurements [*Chelton and Schlax*, 2001].

We have processed the data from the altimeter in the standard manner by removing the geophysical contributions to the signal which we are not interested in (e.g. tides, inverse barometer) and range errors, for example those associated with water vapor in the atmosphere. A complete explanation for altimeter data processing can be found in *Koblinsky et al.* [1998]. The data is derived from the set known as the NASA-Goddard Altimeter Pathfinder [*Koblinsky et al.*, 1998] data set. Prior to averaging into the 2°x 2° boxes, a long temporal mean has been removed from the along track data over all the repeats of a track. Even with such averaging, the RMS error as given by *Chelton and Schlax* [2001], is around 4 cm for low to mid latitudes and closer to 3 cm for latitudes greater than 35°. The satellite tracks converge with increasing latitude near the poles and the sampling becomes more dense and thus, results in smaller RMS errors at these latitudes.

In Figure 1, the black circles define the relative size of the correlations between the model SSH fields binned on a 5°x 5° area, with the closed circles defining correlations greater than 0.5 and the open circles for correlations between 0.4 and 0.5. This plot is shown with 5°x 5° binned correlations, but it should be noted that similar correlations are found when using 2°x 2° bins and when comparing to ERS2 data (35-day repeat cycle giving a denser spatial sampling). While individual locations contain differences, the spatial distribution of where the model correlates highly with the data is similar. That is, the correlations are highest in the north and eastern parts of the basin, along with the tropics and lowest in the more turbulent regions. The ERS2 data covers a much shorter time period than the modeled simulation. These data were averaged on the instrument's 3-day subcycle.

3. Wavelet Analysis

Standard analyses applied to time series to examine dominant signals of variability are Fourier techniques, followed by an examination of the resulting energy spectra for the locations of dominant peaks [*Smith*, 2000]. Such spectra do not provide information on how the localized signal varies in time. Wavelet analysis allows us to look at how the the dominant modes vary temporally. An in depth description of wavelet analysis, the application of it, and a discussion of the significance of the results are given in *Torrence and Compo* [1998]. The method is becoming widely used to analyze a variety of geophysical signals on a wide range of scales. For example, *Gu and Philander* [1995] used the method to examine the ENSO signal. *Meyers et al.* [1993] examined ocean wave dispersion, and others have used the method to analyze wave growth [e.g. *Liu*, 1994].

Similar to windowed Fourier transforms, wavelet analysis allows the localized and dominant frequencies (for which a predetermined scaling can not be defined) to be determined. To begin, given a time series x_n, where *n* = 0 ... *N* -1 and equal temporal spacing, δt , let $W_n(s)$ define the wavelet transform such that

$$W_n(s) = \sum_{n'=0}^{N-1} x_{n'} \psi^* \left[\frac{(n'-n)\delta t}{s} \right], \qquad (1)$$

where (*) indicates the complex conjugate and ψ defines the "wavelet function" which we are using. We construct the wavelet pattern by varying the wavelet scale, s and translating it along the time index n. This pattern shows the amplitude of features verse the scales and how the amplitude changes in time.

ψ, the wavelet function, can be defined in an infinite number of ways, but it must have zero mean and be localized in time and space [*Farge*, 1992]. *Torrence and Compo* [1998] give a detailed discussion on how to choose an appropriate wavelet function. This analysis is done using a Morlet wavelet function, a plane wave modulated by a Gaussian curve where

$$\psi(\eta) = \pi^{-1/4} e^{i\omega\eta} e^{-\eta^2/2}. \qquad (2)$$

Because the chosen wavelet function is complex, the transform $W_n(s)$ is complex. The transform, thus, can reveal both amplitude, $|W_n(s)|$, and phase, $\tan^{-1}[\Im\{W_n(s)\}/\Re\{W_n(s)\}]$ information. The wavelet power spectrum is defined as $|W_n(s)|^2$ and for comparisons, different wavelet spectra are normalized by their variance. This gives a sense of the power relative to white noise.

When determining what portion of the signal is significant, an assumption can be made regarding the redness of the spectrum. *Torrence and Compo* [1998] estimate the background "redness" coefficient (α) for modeling the NINO-3 spectra by calculating the lag-1 and lag-2 coefficients of their data. If

$$x_n = \alpha x_{n-1} + z_n \qquad (3)$$

describes the time series where α is defined as $(R(1) + \sqrt{(}R(2))/2$ and R is the autocorrelation of x and where z_n is a Gaussian white noise addition to the signal, then the mean power spectrum can be defined as

$$P_k = \frac{1-\alpha^2}{1+\alpha^2-2\alpha cos(2\pi k/N)}, \quad (4)$$

where N is the length of the series and k is the spectral point. If a point of the wavelet spectra is greater than the 95% chi-square distribution curve for this mean spectra, the signal is significant. We use a similar method of determining the correlation coefficients to estimate the value of α for the portion of the full signal we are interested in (20 days to 6 months). Overall, our time series are red with the annual signal dominating the spectra. For this study, we concentrate on periods that are shorter than one year. It should, also, be noted that this paper is, primarily, a comparison study rather than a study to definitively identify a set of specific locations where the spectral peaks occur. However, we do attempt to identify these locations for both the T/P data and the simulated fields.

3.1. Comparisons to tide gauges

Wavelet analyses were produced for several of the tide gauges shown in Figure 1 to demonstrate the realism of the model at high frequencies. Figure 2 shows the results of the method when applied to the location at Atlantic City at 38.35°N, 74.42°W; the correlation is 0.75. The wavelet analysis is performed on the time series normalized by its variance resulting in a power spectra in normalized variance units. When determing where the spectra is significant, we have assumed a white noise background ($\alpha = 0$) for the frequencies of interest (0 to 6 months). If a different assumption for the spectra's redness is used, the resulting plot would indicate different areas of significance. The spectral time series on the left side of the Figure 2 can be used to compare the similarity in the signal regardless of the value assigned to α and to examine the differences in absolute magnitudes of the signal in real units.

On the right side, the top panel, Figure 2f and g, show the wavelet spectra in units of normalized power squared (plot shows the log2 of the quantity) for the tide gauge (f) and the model (g). Just above, Figure 2e, is a plot of the two time series, with the tide gauge in gray and the model in black. The time series covers the period of the simulation from 1993 through the end of 1998. The seasonal cycle is evident along with the higher frequency signals. The power spectra show strong similarity between the two time series in both the periods that are enhanced and the temporal variability within the frequency bands. The significant power, as determined by assuming a white noise mean signal, is contoured. Confidence levels are shown by the curved, dashed lines.

To further demonstrate how well the variability of the model across the spectra compares with the tide gauge data, the left side of Figure 2 shows a set of averaged power spectra for various temporal bands, a) centered at 30 days, b) centered at 45.5 days, c) centered at 65.5 days, and d) centered at about 100 days (3 months). Only the 45-day band shows significant difference between the two signals. These band averages show strong similarity in the full signal, regardless of any assumption made about the redness of the spectra and the related significance level (the dashed and dotted lines of the a-d plots). These plots (a-d) of the variance magnitudes show that the model is reproducing the measured variance amplitudes within the chosen bands.

The method is applied further south at Ft. Pulaski, Georgia (32.03°N, 80.9°W) where the model-T/P correlation is 0.77. The high frequency power spectra again shows that the wind driven variability is realistic in the model simulation (Figure 3). At this location there is significantly more energy in the sea surface signal during 1994/5 then during 1997 in the 30 to 40-day band and the 100-day signals. The model's energy is somewhat differently distributed in the 56 to 75-day band than that of the tide gauge.

Both local and remote forcings play a part in the variability of the sea level seen at these coastal stations. At high frequencies, less than 20 days, the wind forcing is highly coherent with the change in the sea level for both the north and south locations and for both the simulated SSH and the in situ fields. The extreme hurricane season of 1995 is reflected in the sea level energy levels for both these stations (Figure 2a and Figure 3a).

At longer periods, for the weak wind period of 1993/1994, there is an increase in energy in the 45-day band for Atlantic City (Figure 2b) but not at the more southerly station, Ft. Pulaski. This period, 1993/1994 period, is defined by *Landsea et al.* [1998] as a "cool" sea surface temperature (SST) phase for the North Atlantic with winds weaker than the mean wind. Suggestions of where the enhanced 45-day SSH signal might come from are given in *Shaw et al.* [1994]. The oscillations may be due to topographical waves generated at a remote location (such as a Gulf Stream ring) or by some locally generated mechanism on the continental slope. Because both the model and the data exhibit similar distributions of energy in this band and because the model does not reproduce Gulf Stream rings which are temporally accurate (see following section), we believe the second explanation. This significant 45-day signal is damped between 1995 and 1997, and then is followed by a peak in the spectra during another relatively weak wind period in 1997.

At lower frequencies, for example, the 100-day band, the southern station at Ft. Pulaski, Figure 3d, shows enhanced energy during the years where the tropical cyclone activity is

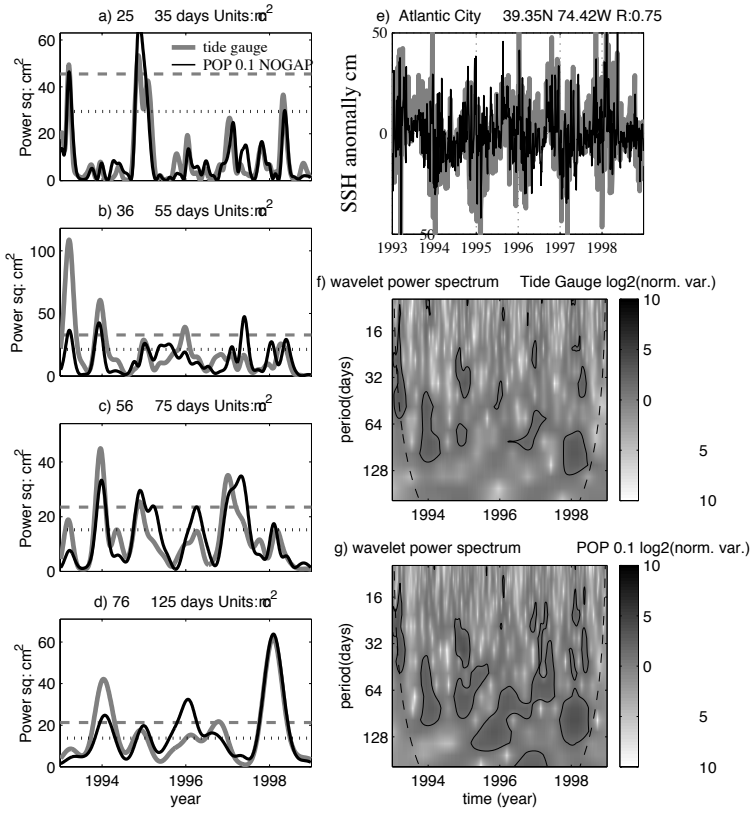

Figure 2. Decomposition of SSH anomaly signal near Atlantic City, NJ, 38.35°N, 74.42°W. a-d) averaged power squared for temporal bands 30 days, 45.5 days, 65.5 days, and 100.5days. e) Time series, at 3 days for the model (black line) and the tide gauge measurements (gray line) - units of cm. f) wavelet power spectrum for tide gauge data in log2(cm^2) units and g) same as f, except for the model. Contoured lines show significant signal at the given periods and the dashed line shows the confidence interval retrieved from the length of the time series.

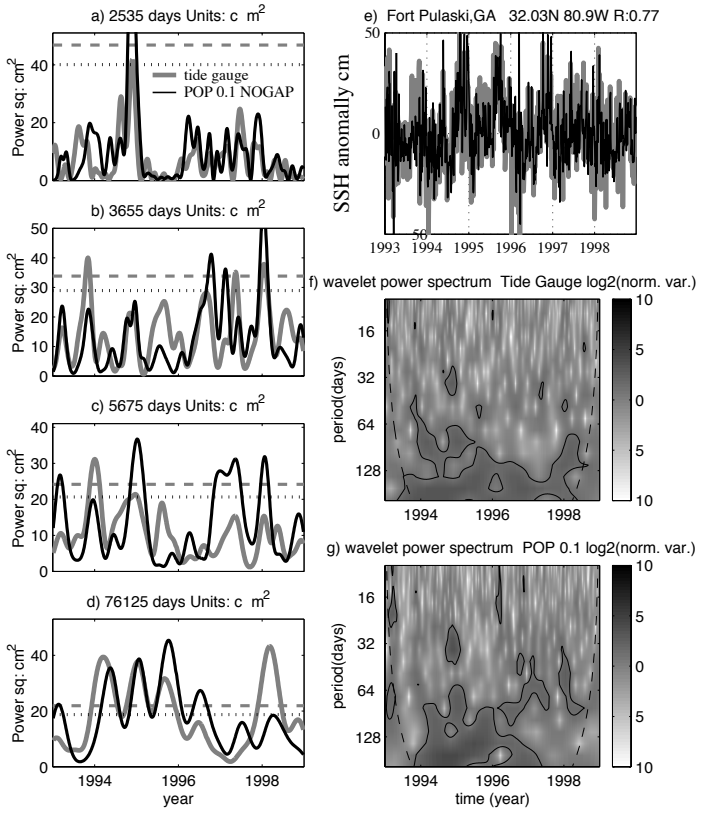

Figure 3. Decomposition of SSH anomaly signal near Ft. Pulaski, GA , 32.02°N, 80.9°W. a-d) averaged power squared for temporal bands 30 days, 45.5 days, 65.5 days, and 100.5 days. e) Time series, at 3 days for the model (black line) and the tide gauge measurements (gray line) - units of cm. f) wavelet power spectrum for tide gauge data in log2(cm^2) units and g) same as f, except for the model. Contoured lines show significant signal at the given periods and the dashed line shows the confidence interval retrieved from the length of the time series.

the greatest, (1995/1996 [*Landsea et al.*, 1998]). The northern station, Atlantic City, is less energetic for this band in both the data and in the modeled fields. It is notable that the model has the ability to reproduce this complicated variability on these short time scales (less than one year).

3.2. Comparisons to buoy temperatures

We selected two NOAA temperature buoy records for comparison to the modeled simulation. The stations are either side of the Gulf Stream Extension. The temperature records are much shorter than the records for the tide gauges. Because the model was only forced with a smooth, daily varying climatological heat flux, this comparison is only making an evaluation of the model's temperature variability due primarily to advection, not local variations in high frequency heat fluxes.

The first wavelet comparisons covers about two years, 1996.5 through 1998.5 at a location north of the Gulf Stream at 41.09°N 66.59°W (see map, Figure 4d). The time series of the temperature anomaly is shown in Figure 4a with the normalized wavelet power spectra for the data and the model, respectively, given in 4b and c; d notes the buoy's location, with respect to the SST field of the model for the day July 1, 1997.

The time series (Figure 4a) shows similarities in the variability on the short temporal scales. For example, near the beginning of the record, there is a large deviation in temperatures, plus and minus 2°C. From the middle of 1997 towards the end of 1997, both records show large deviations from the mean, but at different times. The model, does appear to be simulating some of the variations in the temperature but not always the extreme events. The wavelet analysis shows the strong peak in the observations around late 1997 with a period of around 60 days, the scale of mesoscale eddies. The model is capable of producing such an event, as noted by the peak in the spectrum in Figure 4c around mid 1996 at 60 days. The energy in the periods greater than about 90 days show similar structures, with a loss of significant power in both time series for the 128-day period at around January of both 1997 and 1998.

The second buoy is located to the south of the main path of the Gulf Stream in the model at 34.68°N 72.23°W, Figure 5. The map shows the temperature field of the model for the day January 3, 1998. This time period covers about March of 1996 through mid 1998. The wavelet analysis for these short series shows that the model has again reproduced some of the events, but does not have the energy at the short time periods of less than 60 days that the observations indicate are present again. The dashed lines denote the confidence limits of the observations.

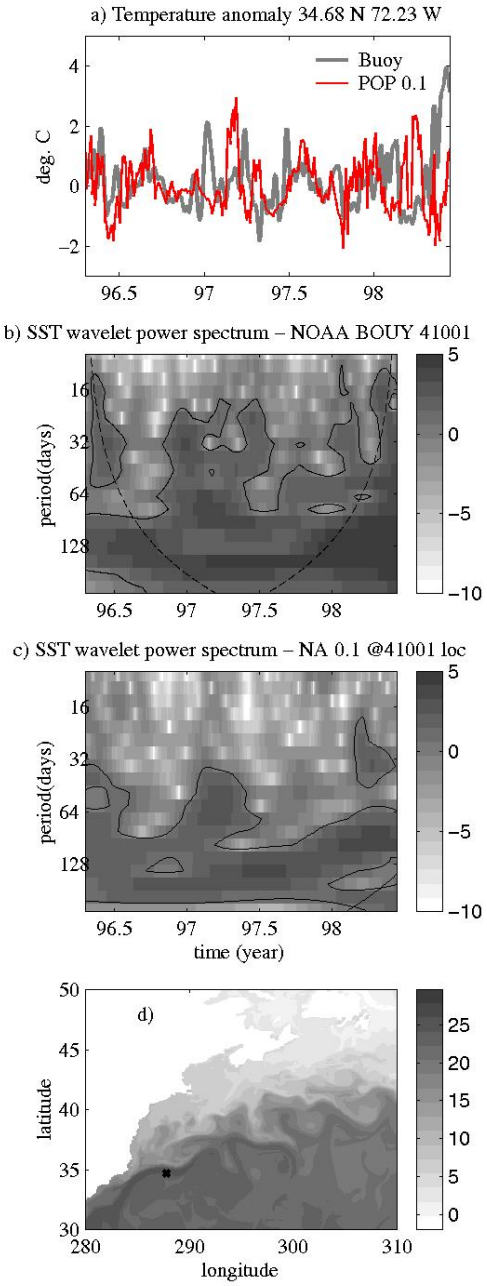

Figure 4. Decomposition of SST anomaly signal at 41.09°N 66.59°W. a) Time series, at 3 days for the model (black line) and the buoy measurements (gray line) - units of °C. b) wavelet power spectrum for buoy data in log2(normalized variance) units and c) same as b, except for the model. Contoured lines show significant signal at the given periods and the dashed line shows the confidence interval retrieved from the length of the time series. d) Map (July 1, 1997) of SST from POP with the buoy location indicated by black dot.

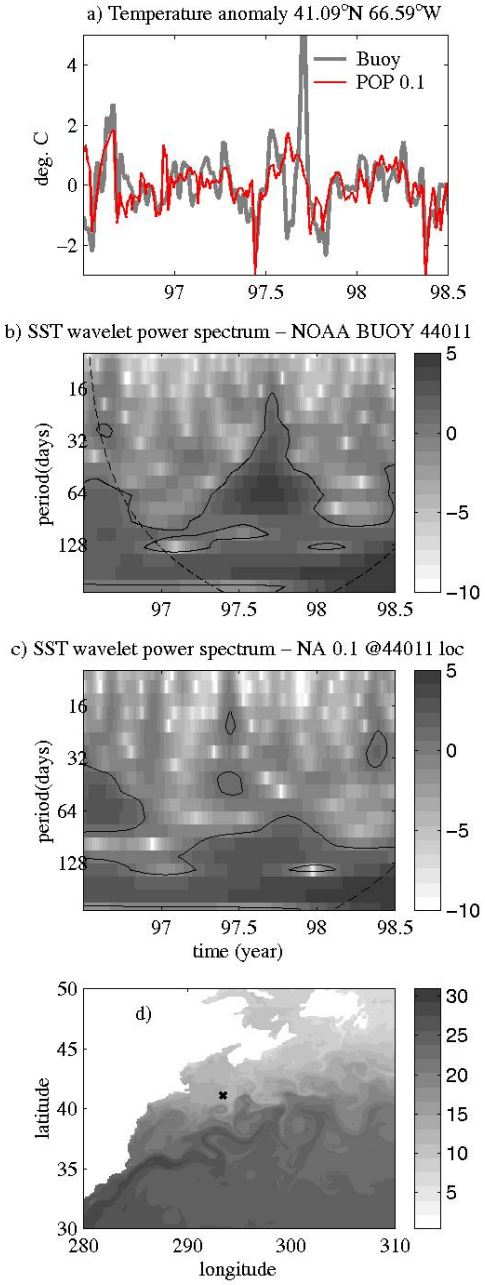

Figure 5. Decomposition of SST anomaly signal at 34.68°N 72.23°W. a) Time series, at 3 days for the model (black line) and the buoy measurements (gray line) - units of °C. b) wavelet power spectrum for buoy data in log2(normalized variance) units and c) same as b, except for the model. Contoured lines show significant signal at the given periods and the dashed line shows the confidence interval retrieved from the length of the time series. d) Map (January 3 1998) of SST from POP with the buoy location indicated by black dot.

3.3. Comparisons to TOPEX/POSEIDON SSH

The wavelet analysis comparison between the model and the altimeter measured SSH are constrained by the sampling of the T/P satellite. In the two previous sections, very localized and daily sampled observations could be compared with the modeled fields. T/P samples at a relatively high rate temporally (every 10 days), but spatially, the sampling requires fields to be averaged over large areas to reduce the error to levels of 3-4cm. The model output for this comparison has been averaged into 2°x 2° bins, resulting in a much-reduced high frequency signal.

Figure 6e shows the time series of the model in black and the T/P SSH anomalies in gray at 42°N, 56°W. The wavelet analysis has again assumed a mean white noise signal ($\alpha = 0$) and the power spectra for the data (T/P) and model are shown in Figure 6f and g, respectively. From the time series, it is easy to observe that the seasonal cycle is captured reasonably well, while the spectra show that the both the data and model contain significant energy at periods greater than around 60 days. Figure 6a-d represent the average power in the bands 35 days, 60 days, 100 days, and about 150 days extracted from the full spectra. For this station, with a relatively high correlation between the model and the T/P data, the comparison (Figure 6f,g) to the data only suggests that the model is simulating what T/P sampled at the lower frequencies. The amplitudes of the signals within the bands are similar, but the phasing is not (for example in Figure 6c and d). And the model shows an enhanced signal for January 1996 (Figure 6d), and likewise, the observed signal in the 150 day band is significant. Neither the model or data show a significant signal in the high frequency band (35 days, Figure 6a).

Further to the north and east, at 62°N and 30°W (southwest of Iceland) Figure 7 shows a somewhat better phase comparison between the model and the observations (Figure 7e). The model's amplitude is much lower than that of the data for the all frequency bands (Figure 7a-d). The phasing within the 150 day band (Figure 7d) is similar between the two time series, with the highest energy levels in the fall of every year. The averaged spectral plot to the right of the wavelet spectra shows that peaks are found in both the modeled fields and the data for 128 days, although in the modeled data, the averaged spectral peak is not significant. Again, because of the large area averages, the model's significant signal is much reduced. At this latitude, the T/P instrument has a much reduced sampling error due to the convergence of its tracks.

Until a more densely sampled altimeter data set is available with similar temporal resolution to that of T/P, the most useful comparison of the wavelet produced spectra over the

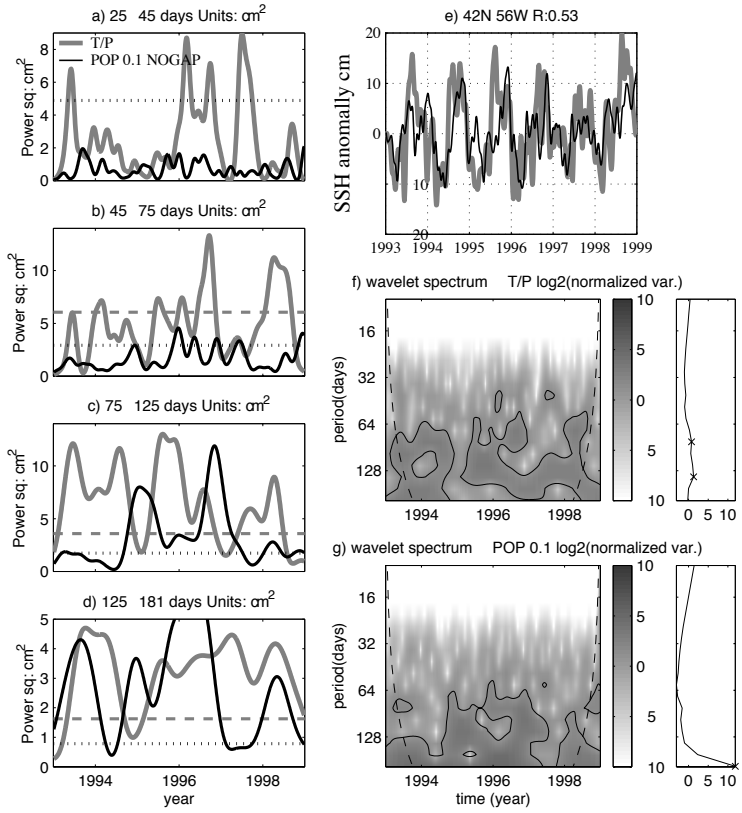

Figure 6. Decomposition of SSH anomaly signal at 42°N 56°W. a-d) averaged power squared for temporal bands 35 days, 55 days, 100 days and 150 days. e) Time series, at 10 days for the model (black line) and the T/P measurements (gray line) - units of cm. f) wavelet power spectrum for T/P data in log2(normalized variance) units and g) same as f, except for the model. Contoured lines show significant signal at the given periods and the dashed line shows the confidence interval retrieved from the length of the time series. The plot to the right of the wavelet spectra is the averaged, detrended spectra value in units of cm^2. The x's mark the spectral peaks.

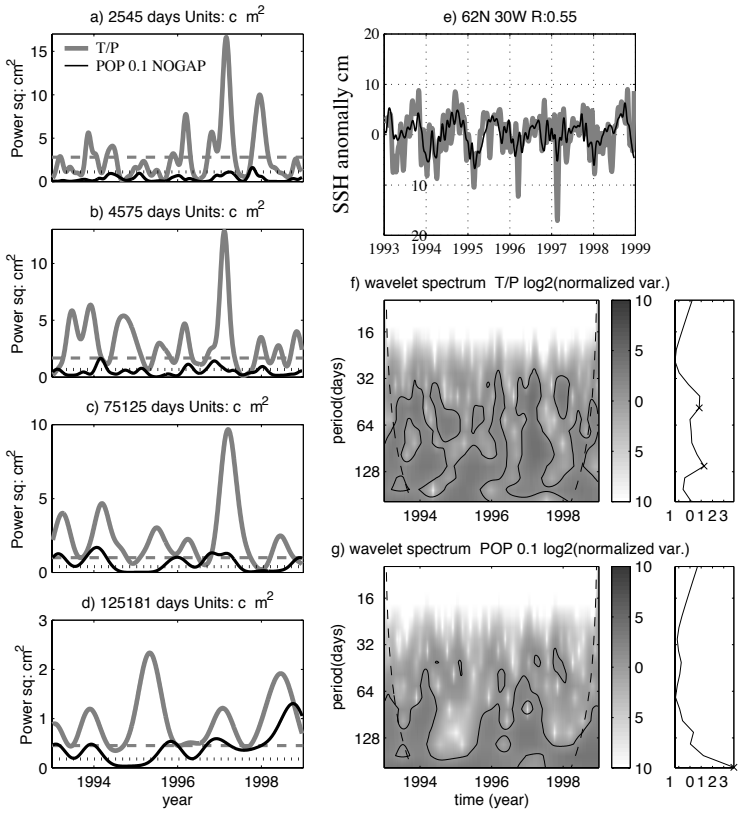

Figure 7. Decomposition of SSH anomaly signal at 62°N 30°W. a-d) averaged power squared for temporal bands 35 days, 55 days, 100 days and 150 days. e) Time series, at 10 days for the model (black line) and the T/P measurements (gray line) - units of cm. f) wavelet power spectrum for T/P data in log2 of normalized variance units and g) same as e, except for the model. Contoured lines show significant signal at the given periods and the dashed line shows the confidence interval retrieved from the length of the time series. The plot to the right of the wavelet spectra is the averaged, detrended spectra value in units of cm^2. The x's mark the spectral peaks.

open ocean areas is to examine the mean spectral values for a given band. Such a calculation is shown in Plate 1. The left set of panels (a-d) are from T/P and the right side (f-h) are from the model. Each map gives the value of the significant mean power for a location and temporal band (a,e 35 days; b,f 60 days; c,g 100 days; d,h 150 days). The color indicates the relative amplitude of the spectral signal for a given band. The circles denote areas that contain a possible peak in the spectral band. The peaks are determined by removing a trend from the global mean spectra (the average of the spectra in time) and then determining which values are one standard deviation above the mean of the detrended mean spectra. Examples of the averaged, detrended spectra values are shown in Figure 6 and Figure 7 to the right of the wavelet power spectra plot. These plots show the peaks defined by the small "x"s. The circles on Plate 1 are not intended to indicate that there is a definitive peak in the spectra for a given band and location, rather to indicate where the spectra has a tendency for a spectral peak.

First, we examine the amplitude of the energy signal in both the model and data (color on Plate 1). In both the model and the T/P, the eastern basin of the Atlantic Ocean is relatively quiet. The model has significant energy in the eastern basin only at periods greater than 45 days. The higher T/P amplitudes in the eastern basin may be due to the sampling and instrument errors of T/P. In the western Atlantic, both show similarities in the location of their mean energies for each band. These plots affirm what has been previously shown in maps of SSH total variance [*Smith et al.*, 2000]. Previous papers on this model [*Smith et al.*, 2000, *McClean et al.*, 2002] have discussed the mislocation of the Gulf Stream and the NAC and the reader is directed to these papers for a discussion of the reasons for the differences.

On close examination, another difference is seen in the two sets of maps with respect to the amplitude. The model shows that there is an increasingly higher amplitude in its energy with lower frequencies (note in particular the energy levels in the NAC region). This is consistent with the description of the wavenumber-frequency spectral plots given in *Smith et al.* [2000, Fig.19] for an area defined as 32°-42°N, 50°- 75°W. The authors state that the model's energy cascade has a steeper slope than the slope calculated from the data. We show that this generally holds throughout the Atlantic.

Next, we examine the locations of the peaks in the spectra (the circles on Plate 1). The two highest frequency bands indicate that both the model and the data show spectral peaks in the area of the Labrador Sea. Examination of the wavelet spectra at 58°N, 56°W. Figure 8 shows that there is significant energy in the 25 to 45-day band during the winter months in both the model and T/P SSH estimates. The wind fields are only somewhat coherent with the height field and only in the 35-day band. Figure 8 also shows that at lower frequencies, the model fields and the observations have a quite different spectra - with a peak in the spectra for the T/P data between 76 and 125 days and no peak, on average, for the simulated fields. The difference might be because the simulation was not forced with interannually varying heat fluxes which may dampen the 35-day signal as exhibited by the observational data and enhance the intraseasonal signal around 90 days.

At lower frequencies, we note that the NAC region in the T/P data indicates peaks in the spectra for periods covering 75 to 125 days (Plate 1c), while the model's energy is dominated by peaks in the 125 to 181-day band (Plate 1h). There is a line of circles defining energy peaks along 20°N in the model fields for the 125 to 181-day band (Plate 1h). These energy peaks are not as clearly defined in the T/P data (Figure 1d) as in the simulation. Plots of time verses longitude of the raw data clearly show that the signal is related to Rossby waves (speed of approximately 6cm/s). The model shows a very distinct propagation pattern; while the pattern is much harder to observe in the T/P data. This is because of the noise in the T/P data. The differences seen below 0° latitude in the 45-75 band may be due to the model being a regional model with the southern boundary condition restored to monthly climatological fields.

4. Discussion and Conclusions

Explanations of causes of the differences between the model fields and the altimeter measurements can be separated, first, into those that are caused by noise or measurement errors within one system or another. Even after averaging over similar 2°x 2° boxes, the altimeter data still contains 3-4 cm of noise and this contributes to the disagreement. Unlike the altimeter we know that the model output is smooth with very low, almost non-existent high frequency noise. Examination of wavelet power series (for example Figure 6a) for the 25 to 45-day band across 35°N (Figure 9) shows distinct, coherent features enhanced in winter time in some years in the model output (Figure 9a) and not in the altimeter data (Figure 9b). One explanation why these are not seen in the altimeter data because they are of the same order as the noise.

Errors in the altimeter data are also caused by aliased high frequency motions [*Stammer et al.*, 2000 and *Tierney et al.*, 2000]. Currently, this signal may be corrected by removing a field estimated from a model. It would be inappropriate to remove it for this study because the field would not be independent of the model data presented here. Also, irregular temporal sampling by the altimeter either by the fundamen-

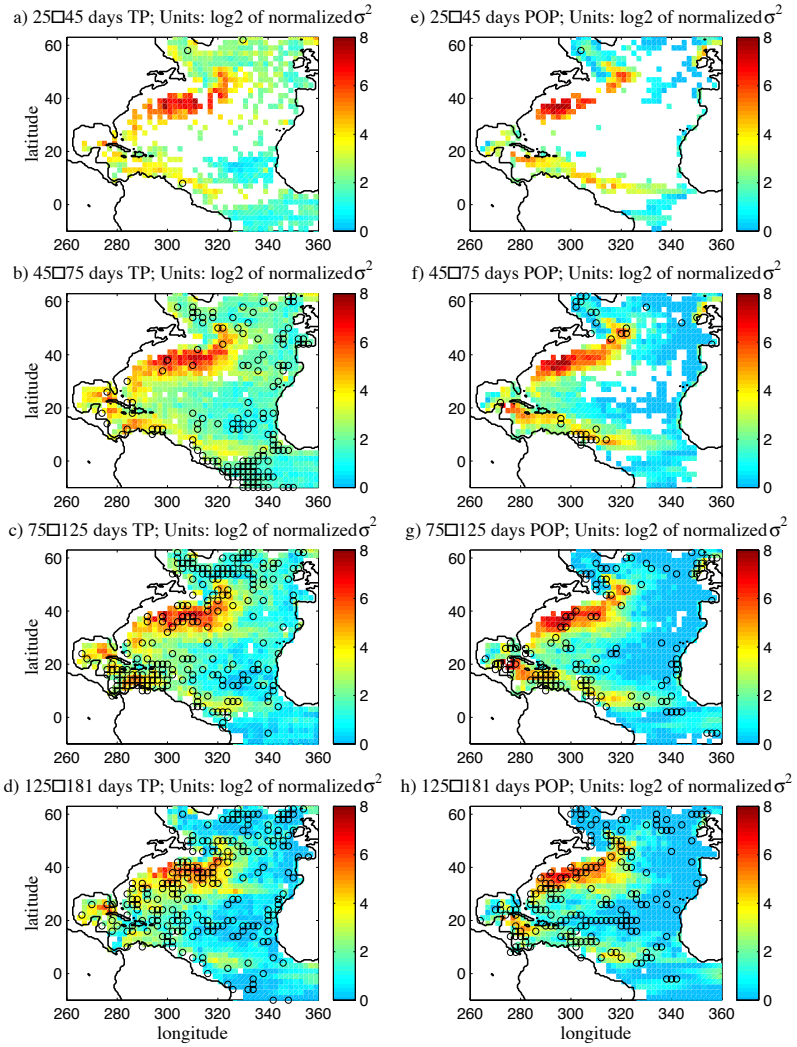

Plate 1. Maps of the mean SSH significant power spectral value for the following spectral bands: a) T/P 25-45 days b) T/P 45-75 days c) T/P 75-125 days, d) T/P 125-181 days e) POP 25-45 days f) POP 45-75 days g) POP 75-125 days, h) POP 125-181 days. Shading is in units of log2(normalized variance). The circles identify locations in which the spectra indicate a possible peak.

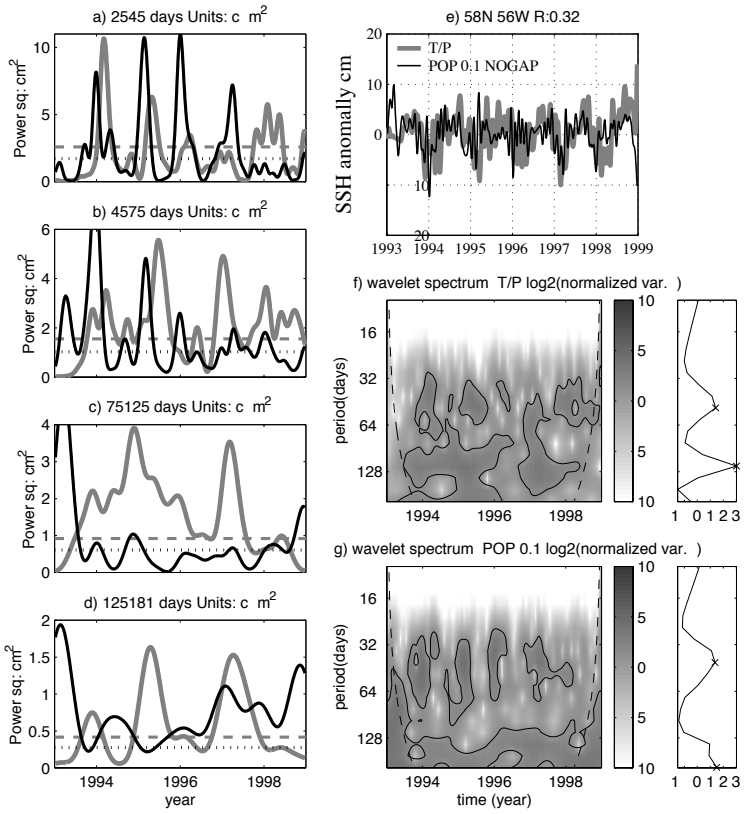

Figure 8. Decomposition of SSH anomaly signal at 58°N 56°W. a-d) averaged power squared for temporal bands 35 days, 60 days, 100 days and 150 days. e) Time series, at 10 days for the model (black line) and the T/P measurements (gray line) - units of cm. f) wavelet power spectrum for T/P data in log2(normalized variance) units and g) same as f, except for the model. Contoured lines show significant signal at the given periods and the dashed line shows the confidence interval retrieved from the length of the time series. The plot to the right of the wavelet spectra is the averaged, detrended spectra value in units of cm^2. The x's mark the spectral peaks.

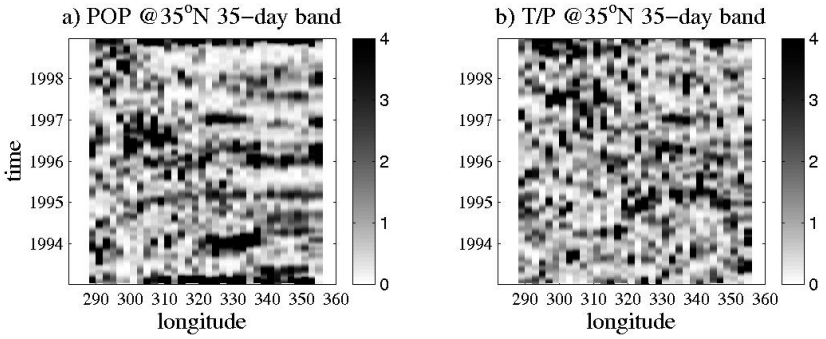

Figure 9. Time-longitude plot of normalized variance of wavelet power at each longitude point along 35°N. The power was normalized by the median power in time for a longitude index. a) POP signal b) T/P signal for the 35-day spectral band. Dark values are relatively high variance.

tal orbit pattern or when the altimeter has not collected the data also contributes to the difference.

For the model, at lower frequencies, within the 125 to 181-day band, incorrect initial conditions may contribute to advective type errors in the model. Wavelet spectra of the difference between the model and the altimeter data within the 125 to 181-day band along 15°N shows a signal similar to what one would expect a Rossby wave to look like (Figure 10). The signal is in the altimeter data (Figure 10b), but not the model fields (Figure 10a). In general, incorrect or incomplete physics within the model may contribute to errors, but would require a local and detailed study to understand the differences and the reasons may be different for different locations.

Last, differences between the model estimates and altimeter estimates may be due to inaccurate surface forcing of the model. Interannual varying heat or freshwater forcing was not included in this model run and to the extent that it may relate to enhancing signals at higher frequencies is left to another study. Differences in the true wind and the estimates given by the meteorological models used to force the model may also account for the differences. This systematic contribution is likely to be small, because the model realistically simulates SSH along the coasts and also appears to do well in the quiescent eastern half of the ocean (see Figure 1).

In summary, a large part of the disagreement is most likely due to the chaotic nature of the mesoscale features in the western half of the basin.

The previous sections have shown and described the realism of the high frequency variability of a primitive equation, 40 level, free surface North Atlantic ocean model simulation at a resolution of 0.1°. We are confident that where the forcing for the model is of high quality (around 1° resolution, daily fields) we are able to simulate the variations of the surface quite well, especially along the eastern coast of the Americas. It is less clear that the high frequency variability (less than 100 days) is simulated well in the middle of the basin. Because of sampling error of 3-4cm of the T/P instrument, we are not able to conclusively quantify the accuracy of the modeled high frequency signal in the areas where only T/P data (and not tide gauge data) is available. We await the time when higher spatially resolved data at a 10-day sample rate is available from the interleaved Jason and T/P satellite system.

From this evaluation, we would like to say something about the confidence that should be placed in the model itself and in the data that may be assimilated at these spatial and temporal resolutions. Using realistic forcing provided by either coupled models or hindcast fields from a meteorological model, we are able to reproduce the high frequency signals, reasonably well in the mean and temporally along the coast where the high frequency (one to six months) SSH variability is, largely, controlled by the local wind forcing. Away from the coast, although there are discrepancies in the phasing of the significant signals, the model does compare reasonably well in amplitude of the energy spectra for various temporal bands.

For purposes of prediction, especially for temporal periods less than a season, assimilation of buoy, drifter, float, and satellite data might enhance a forward model's predictive skill. Much of the research in the assimilation area is focused on how to reduce the size of the matrices that are required in many assimilation techniques. The maps shown in Plate 1 suggest that in quiescent regions of the model, the assimilation of SSH data on scales up to 60 days would not be helpful, because the model does not appear to contain signals that are much more significant than the background noise. In active mesoscale regions, the model does exhibit significant power, but has features displaced in time (see Figure 4) and with increasing energy levels relative to that seen in the T/P data at lower frequencies. We suggest that an efficient method for assimilation would be to only assimilate data into the model where the time derivative of the measurement is greater than the error intrinsic to the measurement (5cm for T/P SSH) itself and in regions where the data contains signals that are significant with respect to the prediction period or smaller.

Acknowledgments. Support for this research has been provided by ONR and NASA, under T/P-Jason SWT. The authors thank NRL (Ruth Preller and Pam Posey) for providing the wind fields. The computing resources were provided for by the Dept. of Defense High Performance Computing Modernization Office, ARL. Thanks go to two anonymous reviewers for their comments and suggestions. Wavelet software was provided by Christopher Torrence and Gilbert Compo and is available at

URL: paos.colorado.edu/research/wavelets

References

Barnier, B., S. Siefridt, and P. Marchesiello, Thermal forcing for a global ocean circulation model using a three-year climatology of ECMWF analyses, *J. of Mar. Sys.*, *6*, 363-380, 1995.

Chao, Y. and L.L. Fu, A comparison between the TOPEX/POSEIDON data and a global ocean general circulation model during 1992-1993, *J. Geophys. Res., 100*, 24965-24976, 1995.

Chelton, D. B., and M.G.Schlax, On the estimation of sea surface height and surface geostrophic velocity from a tandem TOPEX/POSEIDON and Jason-1 altimeter mission, *J. Geophys. Res.*, ,submitted, 2001.

Dukowicz, J. K., and R. D. Smith, Implicit free-surface method for the Bryan-Cox- Semtner ocean model., *J. Geophys. Res.*, *99*,7991-8014, 1994.

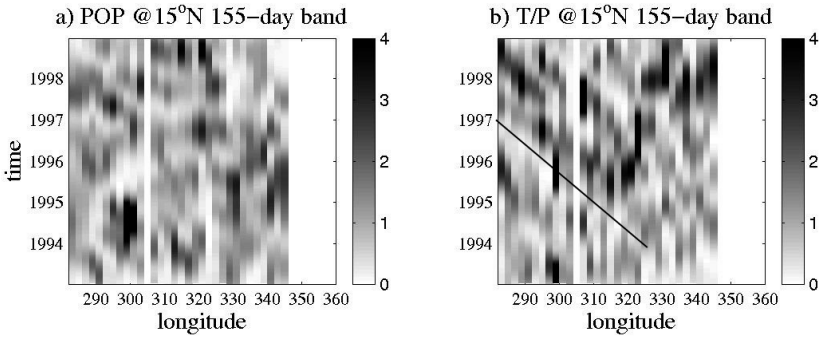

Figure 10. Time-longitude plot of normalized variance of wavelet power at each longitude point along 15°N. The power was normalized by the median power in time for a longitude index. a) POP signal b) T/P signal for the 155-day spectral band. Dark values are relatively high variance.

Farge, M., Wavelet transforms and their applications to turbulence, *Annual Review of Fluid Mechanics*, *24*, 395-457, 1992.

Gu, D., and S. G. H. Philander, Secular changes of annual and interannual variability in the Tropics during the past century., *J. Climate*, *8*, 864-876, 1995.

Koblinsky C. et al., "NASA/GSFC Ocean Pathfinder", http://neptune.gsfc.nasa.gov/ocean.html, 1998.

Kilonsky, B. and P. Caldwell, In the pursuit of high quality SL data, *IEEE Oceans Proceedings*, 2, 669-675, 1991.

Landsea, C. W, R. A. Pielke, Jr., A. M. Mestas-Nuñez, J. A. Knaff, Atlantic basin hurricanes: Indices of climate changes, *Climatic Change*, *42*, 89-129, 1999.

Large, W. G., J. C. McWilliams, and S. C. Doney, Oceanic vertical mixing: a review and a model with a nonlocal boundary layer parameterization. *Rev. Geophys.*, 32, 363-403, 1994.

Liu, P. C., Wavelet spectrum analysis and ocean wind waves, *Wavelets in Geophysics*, E. Foufoula-Georgiou and P. Kumar, Eds., Academic Press, 151-166, 1994.

McClean, J. L, P-M Poulain, J. W. Pelton, and M.E. Maltrud, Eulerian and Lagrangian Statistics from Surface Drifters and a high resolution POP simulation in the North Atlantic", *J. Phys. Oceanogr.*, *32*, 2472-2491, 2002.

Meyers, S. D., B. G. Kelly, and J. J. O'Brien, An introduction to wavelet analysis in oceanography and meteorology: With application to the dispersion of Yanai waves., *Mon. Weather Rev.*, *121*, 2858-2866, 1993.

Semtner, A. J., and R. M. Chervin, Ocean general circulation from a global eddy-resolving model, *J. Geophys. Res.*, *97*, 5493-5550, 1992.

Shaw, P.-T., L. J. Peitrafesa, D. N. Flagg, R. W. Houghton, and Kuo-Hsu Su, Low-frequency oscillations on the outer shelf in the southern Mid-Atlantic Bight, *Deep Sea Res.*, *41*, 253-271, 1994.

Smith, R.D., Maltrud, M. E., Bryan, R. O., and M. W. Hecht, Numerical simulation of the North Atlantic ocean at 1/10° *J. Phys. Oceanogr.*, *30*, 1532-1561, 2000.

Stammer D., Wunsch C., and Ponte, R. M., De-aliasing of global high frequency barotropic motions in altimeter observations. *Geophys. Res. Lett.*, *27*, 1175-1178, 2000.

Tierney, C., Wahr, J., Bryan F., and Zlotnicki, V., Short-period oceanic circulation: implications for satellite altimetry. *Geophys. Res. Lett.*, *27*, 1255-1258, 2000.

Tokmakian, R. T., Comparisons of time series from two global models with tide gauge data, *Geophys. Res. Lett.*, *23*, 3759-3762, 1996.

Torrence, C. and G. P. Compo, A practical guide to wavelet analysis, *Bull. Am. Meteorol. Soc.*, *79*(1), 61-78, 1998.

R. Tokmakian, Department of Oceanography, Naval Postgraduate School, Monterey, California, 93943, USA,email: robint@ucar.edu

Received April 2002; revised Sept 2002; accepted , 2002 .